Article

Comprehensive Parametric Study of a Solar Absorption Refrigeration System to Lower Its Cut In/Off Temperature

Osman Wageiallah Mohammed and Guo Yanling *

College of Mechanical and Electrical Engineering, Northeast Forestry University, Harbin 150000, China; alwagee@rsu.edu.sd
* Correspondence: guo.yl@hotmail.com; Tel.: +86-130-9189-1026

Abstract: Solar-driven ammonia-water absorption refrigeration system (AARS) has been considered as an alternative for the conventional refrigeration and air-conditioning systems. However, its high initial cost seems to be the main problem that postpones its wide spread use. In the present study, a single-stage NH_3/H_2O ARS is analyzed in depth on the basis of energetic and exergetic coefficients of performance (COP and ECOP, respectively) to decrease its cut in/off temperature. This study was carried out to lower the required heat source temperature, so that a less-expensive solar collector could be used. Effects of all parameters that could influence the system's performance and cut in/off temperature were investigated in detail. Presence of water in the refrigerant and evaporator temperature glide was considered. Results revealed that appropriate selection of system's working condition can effectively reduce the driving temperature. Besides, the cut in/off temperature can be significantly decreased by inserting an effective solution heat exchanger (SHX). Required driving temperature can be lowered by up to 10 °C using SHX with 0.80 effectiveness. The results also showed that effects of water content in the refrigerant could not be neglected in studying NH_3/H_2O ARS because it affects both COP and ECOP. Additionally, a large temperature glide in the evaporator can substantially decrease the ECOP.

Keywords: solar assisted cooling; heat pumps; solar thermal systems; absorption refrigeration

1. Introduction

According to the International Institute of Refrigeration, about 15% of total world's electricity generation is consumed for refrigeration and air-conditioning purposes [1]. Approximately 80% of the world's electricity is generated by using fossil fuels that significantly enhance CO_2 emissions, leading to augment the global warming [2]. Furthermore, many developing countries face a shortage of electricity supply [3], particularly during the summer when the need for refrigeration and air-conditioning is obviously increased [4]. On the other hand, many countries enjoy abundant amounts of solar energy, which is freely available throughout the year [5]. To reduce the consumption of fossil fuels and at the same time to promote the use of sustainable energy, exploitation of existing solar energy to operate a refrigeration system is rational. It is quite feasible to harness the solar energy as the demand for cooling and amount of available solar energy are directly proportional to each other [6].

In the field of solar refrigeration, absorption refrigeration seems to be the best option since these systems can be thermally driven by using solar collectors [7]. Advantages of these systems include: use of environment friendly refrigerants, high reliability, extended service life, easy capacity control and efficient and economic use of low-grade energy sources. Absorption refrigeration systems (ARSs) are considered as one of the oldest cooling technologies. These systems essentially work under the same principle as the conventional vapor-compression systems, however, the mechanical compressor is

replaced by a thermal compressor [8]. Main components of a typical absorption system are: generator, condenser, evaporator, absorber and solution pump [9]. To improve the system's performance, usually, two components are added: solution heat exchanger (SHX) and refrigerant heat exchanger (RHX) (Figure 1).

The NH_3/H_2O system can be used for both refrigeration and air-conditioning purposes [10]. The present study concerns a single-stage solar driven ammonia/water absorption refrigeration system (AARS). Use of NH_3/H_2O as working fluid in ARSs remains an attractive application. It performed better than fluorocarbon refrigerants. It is free from limitations imposed by the high freezing temperature of the refrigerant, low crystallization temperature of the solution as in $H_2O/LiBr$ systems and extreme corrosiveness as in ammonia/sodium thiocyanates systems [11,12]. Besides, NH_3/H_2O mixture has zero ozone depletion and zero global warming potentials [13]. Other distinguished benefits include: it can be air cooled, though higher driving temperature is required; and it can freeze water and hence can also store the cold. The only disadvantage of this pair is the volatile nature of water, which is usually overcome by incorporating a rectifier [14]. In the current study, the term strong solution means strong in refrigerant and weak solution indicates weak in refrigerant.

An important parameter that has been neglected in all previous studies in field of solar-driven AARSs is the system's cut in/off temperature. It can be defined as the minimum generator temperature at which the strong solution just starts boiling [15]. This parameter is of paramount importance for solar driven systems. Cut in/off temperature has a major influence on required heating source temperature and hence it determines the operational hours of system during daytime. This temperature, in this way, influences the technical and economic soundness of the system. The cut in/off temperature is mainly affected by the generator pressure and strong solution concentration (X_{ss}). Accordingly, it is also dependent on all sub factors that affect these two parameters such as condenser, evaporator and absorber temperatures, and the pressure losses.

Majority of the simulation models found in the literature for evaluation of AARS are relatively simple. Most of them do not account for the presence of water in refrigerant entering the condenser and evaporator. Due to this water content, evaporation of refrigerant will not be completed without a large temperature glide [16,17]. For example, at evaporator pressure 3.5 bar and refrigerant concentration (X_r) 0.998, the required temperature glide across the evaporator is about 29 °C to achieve complete evaporation. This degree of glide is impractical, so the assumptions of pure refrigerant or saturation vapor at the evaporator outlet can lead to overestimate the system's performance. Few studies discuss the effects of water content in refrigerant. Bogart reported its harmful effects but did not quantify them [18]. Fernandez-Seara and Sieres analyzed the effect of water content on the system's coefficient of performance (COP) but its effect on the exergetic performance was not included in their studies [16,19]. Táboas et al. [20] considered a temperature glide of 10 K in evaporator to reduce the amount of liquid refrigerant that was not evaporated and consequently increased cooling effect and COP. However, the effect of this large temperature glide on exergetic coefficient of performance (ECOP) was not reported in that study.

In last decades exergy analysis gained more attention and has been widely applied to show how the system effectively utilizes given energy resources [21]. Then, it could be decided which system's component need further improvement to reduce irreversibility [22,23]. Knowledge of ECOP can give idea whether the system should be more improved or not. In current comprehensive study, a single-stage solar driven NH_3/H_2O ARS is put under detailed consideration. The main objective of this study is to decrease driving temperature (cut in/off temperature) of the system. It is analyzed on the basis of energetic and exergetic coefficients of performance (COP and ECOP), circulation ratio (CR), electric power consumed by solution pump (W_{pump}) and components' thermal loads. In the present model, effects of water content in refrigerant through the condenser and evaporator are taken into account. All parameters that can affect the system's cut in/off temperature have been investigated. Effect of preheating the strong solution on reducing the cut in/off temperature is also examined in

this study. Besides conventional parameters, special attention has been paid to see the effects of temperature glide in evaporator and SHX effectiveness.

2. System Description

The system consists of a solar thermal collector linked to a single-stage NH$_3$/H$_2$O absorption chiller as shown in Figure 1. Hot water from solar collector is used to heat the strong solution in generator to produce ammonia vapor at high pressure. During the process, some water vapor is also generated and passes with the ammonia vapor to rectifier (3). Function of the rectifier is to reduce water content in NH$_3$ vapor. High concentrated NH$_3$ vapor enters the condenser (5), where it is condensed and then collected in receiver (6). Afterwards, liquid refrigerant passes through reflux valve which divides the flow into two streams: the first stream (7) represents a small fraction of liquid refrigerant, which returns to rectifier by means of reflux; and the second stream (8) passes through refrigerant heat exchanger (RHX) where it is sub-cooled by refrigerant vapor leaving the evaporator (11). Sub-cooled liquid (9) passes through expansion valve (10) to evaporator, where it is evaporated at low pressure and temperature to induce cooling effect. The evaporated refrigerant enters absorber (12) after passing through RHX. In absorber the vapor is absorbed by weak solution returning from generator through solution heat exchanger SHX. Pressure of weak solution is reduced by an expansion valve before entering the absorber from generator pressure to absorber pressure. The purpose of using SHX is to preheat the strong solution and to precool the weak solution before entering the absorber [24]. An electric-driven pump is used to boost the strong solution pressure coming from absorber and leading to the generator. Water is used to cool both the condenser and the absorber. To achieve this, two additional pumps and fans (termed as auxiliaries) are employed.
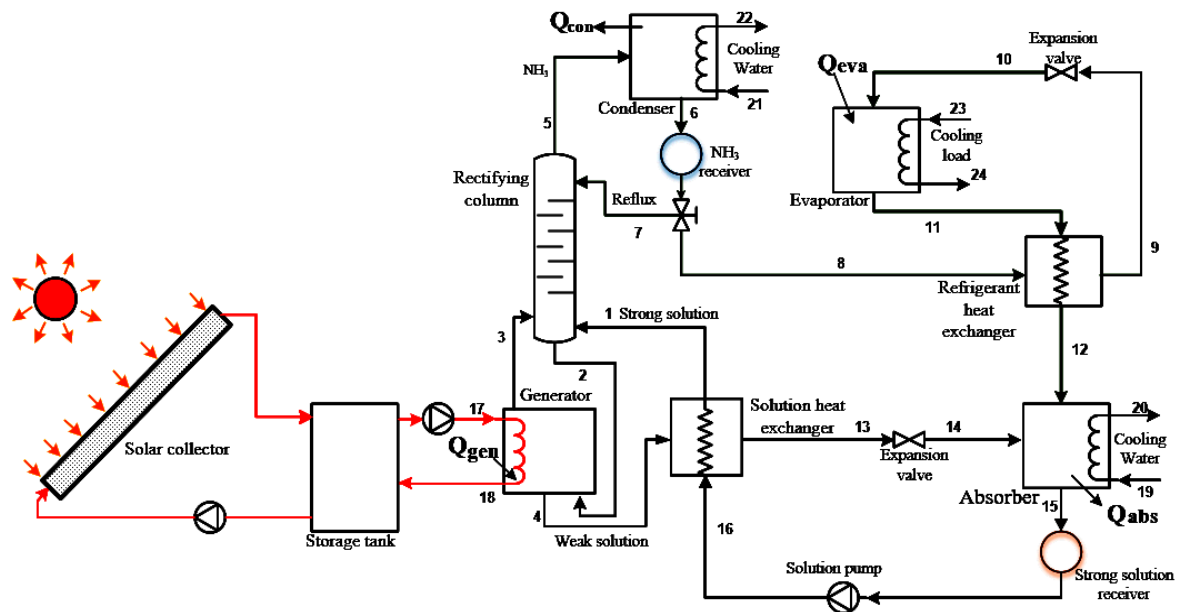

Figure 1. Single-stage NH$_3$/H$_2$O solar absorption refrigeration system.

3. System Modeling

A simulation model was developed to evaluate the performance of a single-stage NH$_3$/H$_2$O ARS. The developed model is based on energy, mass and species conservation equations. General forms of these equations are specified as [4,7]:

Energy conservation-

$$\sum(\dot{m}h)_{in} - \sum(\dot{m}h)_{out} + \left[\sum\dot{Q}_{in} - \sum\dot{Q}_{out}\right] \pm W = 0 \tag{1}$$

Mass conservation-

$$\sum \dot{m}_{in} - \sum \dot{m}_{out} = 0 \tag{2}$$

Species conservation-

$$\sum (\dot{m}x)_{in} - \sum (\dot{m}x)_{out} = 0 \tag{3}$$

Exergy balance-

$$\sum \dot{E}_{in} - \sum \dot{E}_{out} + \sum \left(1 - \frac{T_o}{T_j}\right) \dot{Q}_j = \sum \dot{E}_{dest} \tag{4}$$

By applying these general forms to each individual component in the system, energy and exergy balances can be written as following:

$$\dot{Q}_{gen} = \dot{m}_3 h_3 + \dot{m}_4 h_4 - \dot{m}_2 h_2 \tag{5}$$

$$\dot{E}_{dest,\, gen} = \dot{m}_2 E_2 - \dot{m}_3 E_3 - \dot{m}_4 E_4 + \dot{Q}_{gen}\left[1 - (T_o/T_{gen})\right] \tag{6}$$

$$\dot{m}_2 h_2 + \dot{m}_5 h_5 = \dot{m}_1 h_1 + \dot{m}_3 h_3 + \dot{m}_7 h_7 \tag{7}$$

$$\dot{E}_{dest,\, rect} = \dot{m}_1 E_1 + \dot{m}_3 E_3 + \dot{m}_7 E_7 - \dot{m}_2 E_2 - \dot{m}_5 E_5 \tag{8}$$

$$\dot{Q}_{cond} = \dot{m}_5 h_5 - \dot{m}_6 h_6 \tag{9}$$

$$\dot{E}_{dest,\, cond} = \dot{m}_5 (E_5 - E_6) - \dot{Q}_{cond}\left[1 - (T_o/T_{cond})\right] \tag{10}$$

$$\dot{Q}_{RHX} = \dot{m}_8 (h_8 - h_9) = \dot{m}_r (h_{12} - h_{11}) \tag{11}$$

$$\dot{E}_{dest,\, RHX} = \dot{m}_8 (E_8 - E_9 + E_{11} - E_{12}) \tag{12}$$

$$\dot{Q}_{eva} = \dot{m}_8 (h_{11} - h_{10}) \tag{13}$$

$$\dot{E}_{dest,\, eva} = \dot{m}_8 (E_{10} - E_{11}) + \dot{Q}_{eva}\left[1 - (T_o/T_{eva})\right] \tag{14}$$

$$\dot{Q}_{abs} = \dot{m}_{12} h_{12} + \dot{m}_{14} h_{14} - \dot{m}_{15} h_{15} \tag{15}$$

$$\dot{E}_{dest,\, abs} = \dot{m}_{12} E_{12} + \dot{m}_{14} E_{14} - \dot{m}_{15} E_{15} - \dot{Q}_{abs}\left[1 - (T_o/T_{abs})\right] \tag{16}$$

$$\dot{Q}_{SHX} = \dot{m}_4 (h_4 - h_{13}) = \dot{m}_{16} (h_1 - h_{16}) \tag{17}$$

$$\dot{E}_{dest,\, SHX} = \dot{m}_4 (E_4 - E_{13}) + \dot{m}_{16} (E_{16} - E_1) \tag{18}$$

where T_o is the reference temperature taken as 25 °C.

The reflux ratio is defined as:

$$Reflux = \frac{\dot{m}_7}{\dot{m}_6} = \frac{\dot{m}_7}{\dot{m}_7 + \dot{m}_8} \tag{19}$$

$$\varepsilon_{RHX} = \frac{T_8 - T_9}{T_8 - T_{11}} \tag{20}$$

$$\varepsilon_{SHX} = \frac{T_4 - T_{13}}{T_4 - T_{16}} \tag{21}$$

where ε_{RHX} and ε_{SHX} are effectiveness of RHX and SHX, respectively.

Electric power consumed by solution pump can be given by:

$$W_{pump} = \frac{\dot{m}_{15} v_{15} (P_{16} - P_{15})}{\eta_{pump}} \tag{22}$$

Here, ν is the specific volume of solution (m^3/kg), and η_{pump} is the pump overall efficiency. Equation (22) gives basic power required for pumping the working solution. However, additional power is needed to run the auxiliaries (fans and cooling water pumps). Palomba et al. [25] recently reported that the power consumed by auxiliaries in AARS can be estimated as 23 W/kW$_{cooling}$. Hence, for a system with 100 kW cooling power, the auxiliaries' power will be 2.3 kW.

System analysis is carried out based on following assumptions:

- Vapor at the rectifier outlet is saturated at its pressure and mass concentration.
- Rectifier has a constant efficiency.
- Refrigerant, which passes through the condenser, evaporator and RHX, is a mixture of water/ammonia with a specific concentration, so that effects of water presence in refrigerant can be quantified.
- Condensation through the condenser is complete.
- Refrigerant at condenser outlet is saturated liquid at condenser temperature.
- Strong solution at absorber outlet is saturated and it is at absorber temperature.
- Expansion valves are adiabatic.
- Weak solution leaves generator at its temperature.

Some parameters used in this study were taken from previous studies at their practical values [20,24]. Therefore, for the system at base condition; ε_{SHX} = 0.80, ε_{RHX} = 0.80 and pump efficiency is 0.65. Minimum reflux ratio is taken as 0.2 to obtain a refrigerant with a concentration 0.998. Temperature of heating source decreases by 10 °C across the generator. Pressure loss between evaporator and absorber is taken as $\Delta P/P$ = 0.075 and $\Delta P/P$ = 0.05 between the generator and condenser where P is pressure at the pipe exit.

Performance of ARSs is usually measured by COP, ECOP and CR of the system. The COP of ARS is given by:

$$\text{COP} = \frac{Q_{eva}}{Q_{gen} + W_{pump}} \tag{23}$$

and the ECOP is given by:

$$\text{ECOP} = -\frac{Q_{eva}\left(1 - T_o/T_{eva}\right)}{Q_{gen}\left(1 - T_o/T_{gen}\right) + W_{pump}} \tag{24}$$

The circulation ratio is given as:

$$\text{CR} = \frac{\dot{m}_1}{\dot{m}_8} \tag{25}$$

3.1. Simulation Tool

The simulation software Cycle-Tempo was used to compute energy and mass balances in all components of the system. The components have been assembled graphically in the software scheme window as depicted by Figure 2. Necessary data were entered, followed by the simultaneous solution of energy and mass balances equations to obtain energy, exergy and mass flows through all components and pipes. Values for temperature, pressure, enthalpy, entropy, vapor quality and mass fraction at all points (points 1–24) have been specified. Thermodynamic properties of working fluid were obtained from equations of Ziegler and Trepp, implemented in the software [26].
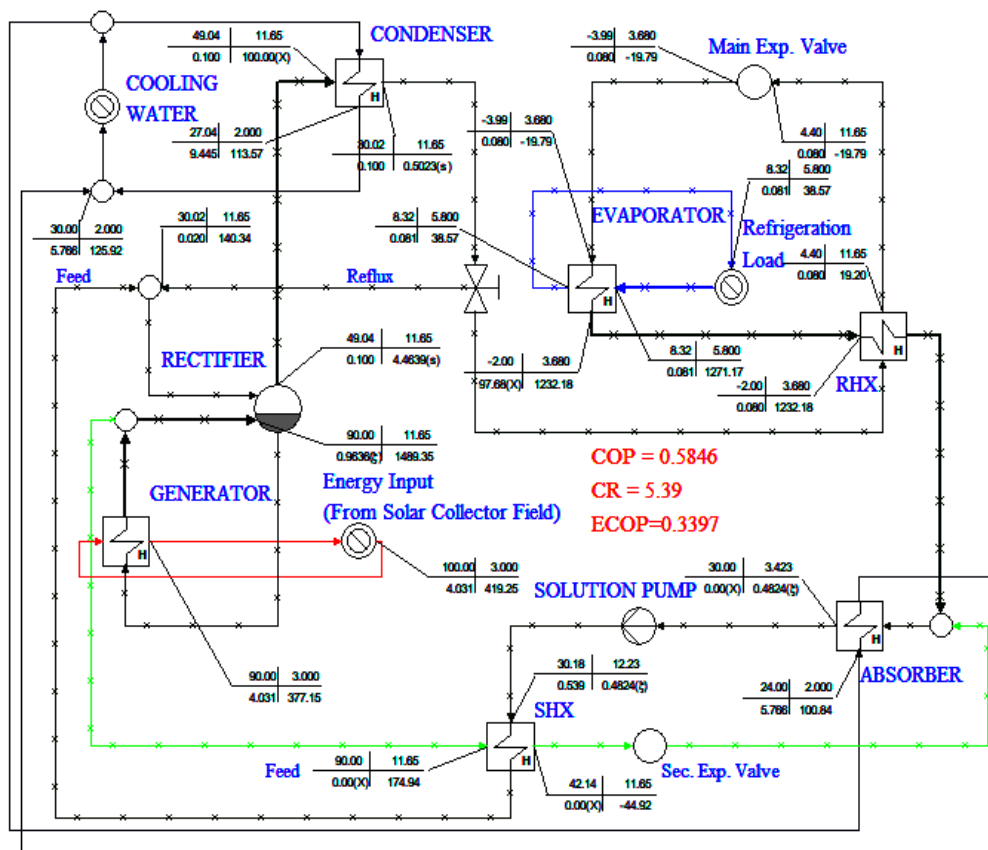
Figure 2. Single stage NH_3/H_2O absorption system in Cycle-Tempo scheme window.

3.2. Model Validation

The simulation model was validated by using two sets of experimental data. First set is experimental results for a commercial solar driven unit (chilli® PSC 10 from SolarNext Company) published in [27]. Second one results from an experimental study conducted by Mendes and Pereira [28] and reported in [29]. Comparison between several key values computed by the model and those published in the cited references is presented in Table 1. As shown, results of the model are close to that in mentioned references.

Table 1. (**a**) Results of model validation using data from Ref. [27]; and (**b**) results of model validation using data from Ref. [29].

(a)							
Stream No.	Temperature (°C)			Energy Flow (kW)			
	Ref. [27]	Model	Difference (%)	Quantity	Ref. [27]	Model	Difference (%)
1	62	62	0.00	$\dot{Q}_{gen}$	17.1	16.6	−2.9
2	69	72.6	5.2	$\dot{Q}_{con}$	9.6	9.8	2.1
3	79	79	0.00	$\dot{Q}_{eva}$	10.5	10.14	−3.4
4	70	70	0.00	$\dot{Q}_{abs}$	15.9	14.6	−8.2
5	64	66	3.1	COP	0.60	0.60	0.00
6	30	30	0.00				
8	31	31	0.00	External Flows (kg/s)			
10	8	8	0.00	Quantity	Ref. [27]	Model	Difference (%)
11	11	11	0.00	$\dot{m}_{17,18}$	0.52	0.52	0.00
12	11	11.2	1.8	$\dot{m}_{19,20}$	0.56	0.56	0.00
13	30	30.6	2	$\dot{m}_{21,22}$	0.33	0.33	0.00
14	30	30.7	2.3	$\dot{m}_{23,24}$	0.82	0.772	5.9
15	25	25	0.00				
16	25	25.2	0.8				
17	86	86	0.00				
18	79	78.4	0.8				
19	22	22	0.00				
20	31	29.8	−0.6				
21	22	22	0.00				
22	31	30.9	0.3				
23	15	15	0.00				
24	19	19	0.00				

(b)							
Stream No.	Temperature (°C)			Energy Flow (kW)			
	Ref. [29]	Model	Difference (%)	Quantity	Ref. [29]	Model	Difference (%)
1	91.9	93	1.2	$\dot{Q}_{eva}$	5.0	5.0	0.00
4	104	104.3	0.3	$\dot{Q}_{gen}$	8.96	8.66	−3.3
5	94	93.7	−0.3	$\dot{Q}_{con}$	5.94	5.68	−4.4
6	46.7	46.8	0.2	$\dot{Q}_{abs}$	8.11	7.97	−1.7
9	14.3	14.8	2.1	$\dot{Q}_{SHX}$	11.42	11.71	2.5
10	7.3	7.3	0.00	$\dot{Q}_{RHX}$	0.74	0.70	−5.4
11	12.3	12.3	0.00	COP	0.55	0.56	1.8
12	31.3	33.8	8				
13	54.6	54.5	−0.2				
14	54.8	54.6	−0.4				
15	46.9	46.9	0.00				
16	47.1	47.3	0.4				

4. Results and Analysis

By running the simulation model, effects of all operating parameters on system's performance were obtained. For different working conditions, coefficient of performance (COP), exergetic coefficient of performance (ECOP), cut in/off temperature, circulation ratio (CR), power consumed for solution pumping (W_{pump}) and the different components' thermal loads were determined. Results are presented graphically by varying parameter under consideration while keeping remaining parameters at their base condition values. Consequently, different possible design points have been compared. In this study, the system base condition is considered at T_{gen} = 90 °C, T_{con} = T_{abs} = 30 °C, T_{eva} = −4 °C, the reflux ratio = 0.2 and the strong solution concentration (X_{ss}) by mass = 0.4824. The system cooling capacity ($\dot{Q}_{eva}$) is always 100 kW. Due to water presence in refrigerant, some degree of temperature glide through evaporator is required. Therefore, in all coming subsections, temperature glide between evaporator entrance and exit is equal to 2 °C. Consequently, more refrigerant can be evaporated.

This degree of glide was taken in accordance with the results presented in Section 4.7 and experimental outcomes reported in [27]. Table 2 displays results of thermodynamic analysis of the system under base condition. Numbers here refer to the points in Figure 1. Predicted performance results are also presented in same table. Values of working parameters and their simulation ranges are summarized in Table 3.

Table 2. Results of system analysis at base condition.

Point No.	Temperature (°C)	Pressure (bar)	Flow (kg/s)	NH_3 Conc. (By Mass)	Enthalpy (kJ/kg)	Entropy (kJ/kg·K)
1	66.2	10.84	0.420	0.500	56.74	0.7747
2	64.6	10.32	0.427	0.500	49.07	0.7517
3	90.0	10.32	0.099	0.957	1501.93	4.9729
4	90.0	10.32	0.328	0.362	180.38	1.1077
5	46.2	10.32	0.115	0.998	1344.16	4.5167
6	26.0	10.32	0.115	0.998	120.87	0.4384
7	26.0	10.32	0.023	0.998	120.87	0.4384
8	26.0	10.32	0.092	0.998	120.87	0.4384
9	4.3	10.32	0.092	0.998	18.66	0.0838
10	−5.3	3.50	0.092	0.998	−25.69	−0.0750
11	−5.0	3.50	0.092	0.998	1061.73	3.9837
12	−4.7	3.50	0.092	0.998	1163.94	4.3649
13	39.4	10.32	0.328	0.362	−51.94	0.4187
14	39.5	3.50	0.328	0.362	−51.94	0.4212
15	26.0	3.26	0.420	0.500	−126.18	0.2040
16	26.7	10.84	0.420	0.500	−124.74	0.2057

$\dot{Q}_{gen}$ = 187 kW	$\dot{Q}_{con}$ = 140.6 kW	$\dot{Q}_{eva}$ = 100 kW	$\dot{Q}_{RHX}$ = 9.4 kW
$\dot{Q}_{abs}$ = 143 kW	$\dot{Q}_{SHX}$ = 76.3 kW	$\dot{W}_P$ = 1.01 kW	CR = 3.65
COP = 0.5316	ECOP = 0.3243		

Table 3. Base values for system's parameters and their simulation ranges.

Parameter	Base Value	Simulation Range
Strong solution concentration (X_{ss}) by mass	48.24%	41–58 (%)
Refrigerant concentration	99.8%	98.6–99.9 (%)
Generator temperature (T_{gen})	90 °C	74–120 (°C)
Condenser temperature (T_{con})	30 °C	20–42 (°C)
Evaporator temperature (T_{eva})	−4 °C	−12–12 (°C)
Absorber temperature (T_{abs})	30 °C	15–42 (°C)
Evaporator temperature glide	2 °C	0.0–14 (°C)
Reflux ratio	0.2	0.0–0.80
Solution heat exchanger effectiveness (ε_{SHX})	0.80	0.0–1
Refrigerant heat exchanger effectiveness (ε_{RHX})	0.80	not changed
Solution pump efficiency (η_{pump})	0.65	not changed
Cooling power (Q_{eva})	100 kW	not changed
Minimum temperature difference in the generator	10 °C	-
Minimum temperature difference in the condenser	6 °C	-
Minimum temperature difference in the absorber	6 °C	-
Minimum temperature difference in the evaporator	10 °C	-
Minimum temperature difference in the SHX	12 °C	-
Minimum temperature difference in the RHX	6 °C	-
Cooling water temperature	24 °C	-
Auxiliaries' power	2.3 kW	-

4.1. Effect of Strong Solution Concentration (X_{ss})

X_{ss} is an important parameter in AARSs. Performance of the system is highly improved as ammonia concentration increases in the solution entering generator. This improvement occurs because more refrigerant can be released in generator, which leads to lower CR and thermal loads. As appeared in Figure 3, both COP and ECOP increase as the percentage of ammonia in strong solution increases. Initially, both COP and ECOP rise sharply with increase in X_{ss}. It proceeds as such until the percentage

of ammonia reaches at about 48%. Afterwards, the increase in COP and ECOP is at a lower rate. X_{ss} also affects the CR noticeably, as illustrated by Figure 4. The CR decreases abruptly as ammonia percentage increases in start, afterwards the decrease of CR continues but at a lower ratio.

Another important parameter affected by the X_{ss} is the cut in/off temperature. Figure 4 expresses the relation between cut in/off generator temperature and X_{ss}. As shown, at constant generator pressure, cut in/off temperature is inversely influenced by ammonia concentration in the solution entering generator. Amount of electric power consumed by solution pump (W_{pump}) is directly proportional to the value of circulation ratio. Therefore, increase of strong solution concentration has a positive impact on reducing the required pumping power as shown by Figure 5. Figure 6 implies the variations of components' thermal loads at different X_{ss}. As illustrated, for constant Q_{eva}, the Q_{gen}, Q_{abs} and Q_{SHX} fall rapidly (due to decrease in the CR) as the ammonia concentration increases. Later, the decrease of thermal loads is noticed at a low rate, while Q_{con} and Q_{RHX} remain unchanged. In addition, it is clear that Q_{SHX} is very sensitive to the change in X_{ss}. To lower the system's initial cost, size of components (depend on thermal load) should be minimized. Hence, X_{ss} has an important impact on the system's cost. However, the use of strong solution with higher concentration requires lower absorber temperature which is limited by temperature of available cooling water (or air).
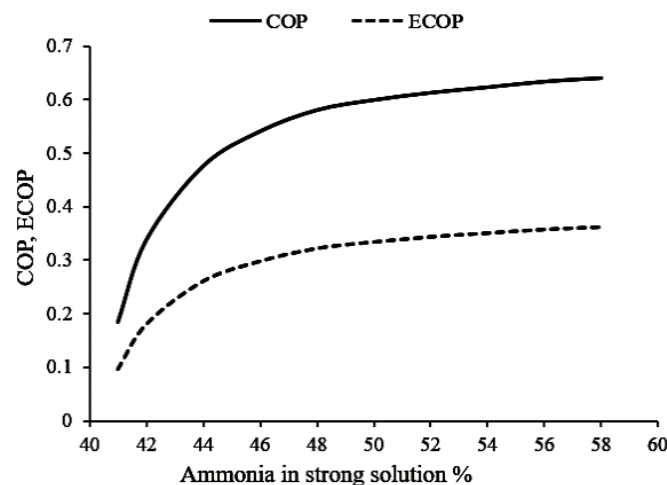
Figure 3. Effect of X_{ss} on energetic and exergetic coefficients of performance (COP and ECOP).
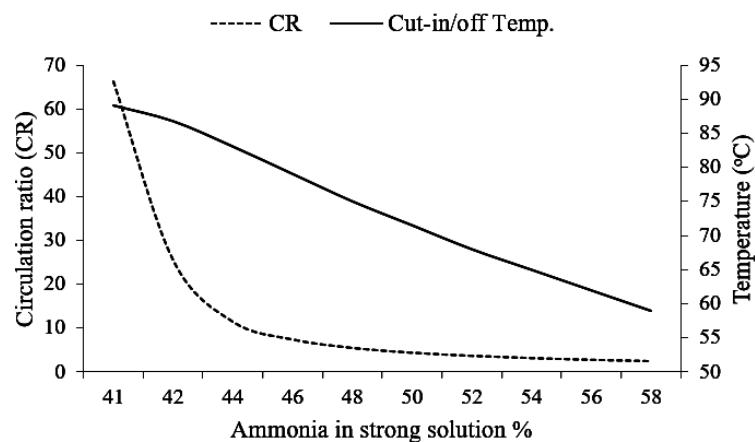

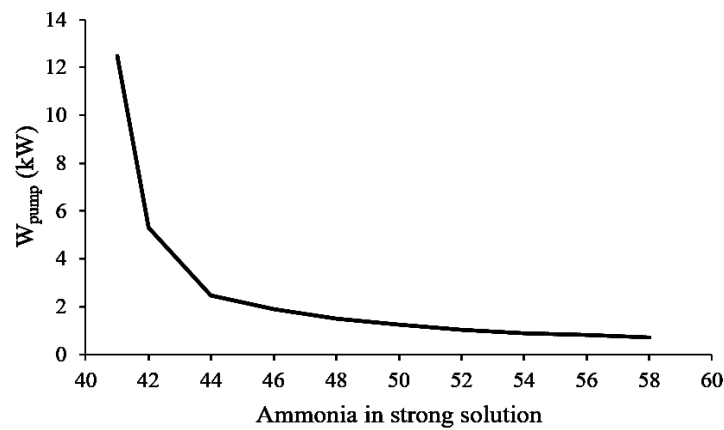**Figure 4.** Effect of X_{ss} on circulation ratio (CR) and cut in/off temperature.

Figure 5. Effect of X_{ss} on pumping power.
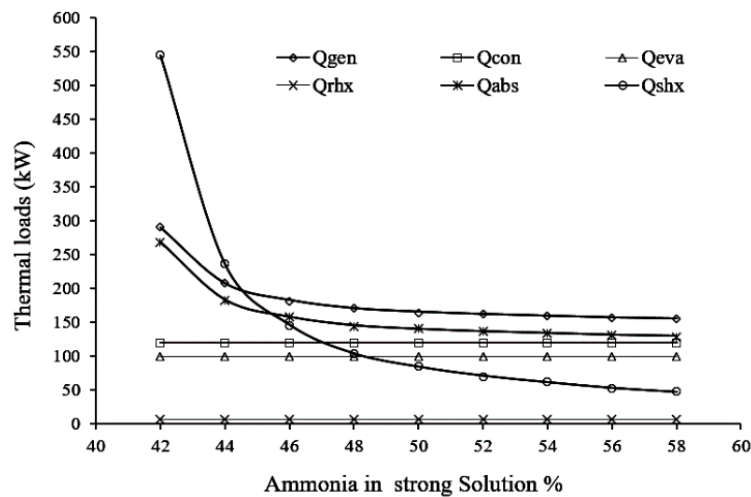

Figure 6. Variations of thermal loads with X_{ss}.

4.2. Effect of Generator Temperature (T_{gen})

Generator temperature (T_{gen}) is one of the most important parameters affecting the performance of absorption systems. The COP and ECOP of system under consideration were plotted as functions of T_{gen} in Figure 7. The T_{gen} varied from cut in/off limit to 120 °C, keeping all other parameters constant at their base values except heating water temperature. As T_{gen} rises from cut in/off value, the COP rapidly increases until about 90 °C; after that, gradient of COP curve becomes nearly flat. Meanwhile, ECOP passes through maxima at 86 °C and drops gradually after that. This suggests that exergetic performance of the system is affected more by increasing T_{gen} than energetic performance. This behavior can be attributed to the increase of solution temperature in generator and absorber which leads to more exergy losses in two components. These results are consistent with those reported by other authors [4,20].
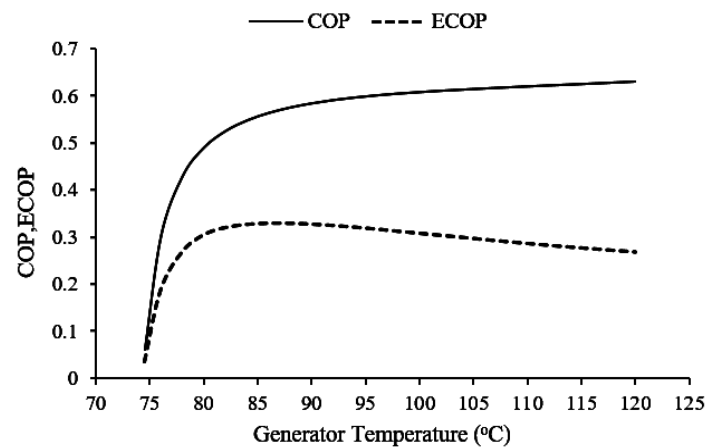
Figure 7. Effect of T_{gen} on COP and ECOP.

The generator at a higher temperature can produce more ammonia vapor, so CR declines rapidly as T_{gen} increases until 80 °C. Later, the gradient of CR curve becomes nearly flat, as depicted in Figure 8. Identical behavior is noted for the required pumping power, as portrayed in Figure 9. For the system designed to work at T_{gen} = 80 °C, the pump power is 2.75 kW. This value is reduced to 1.34 kW for T_{gen} = 90 °C. On the other hand, as T_{gen} arises, the refrigerant concentration in vapor leaving generator and entering rectifier descends. Resultantly, a rectifier with higher efficiency is required which means adding more costs. The relation between T_{gen} and NH_3 concentration in vapor from generator is shown in Figure 8. At T_{gen} = 80 °C, ammonia concentration in vapor is 0.9792, which decreases to only 0.8593 at T_{gen} = 120 °C due to evaporation of more water at higher T_{gen}. Furthermore, T_{gen} affects Q_{gen}, Q_{abs} and Q_{SHX}, as described in Figure 10. When T_{gen} ascends, the thermal loads of the three components decrease. Moreover, it can be seen that Q_{SHX} is most sensitive to the change of T_{gen}.
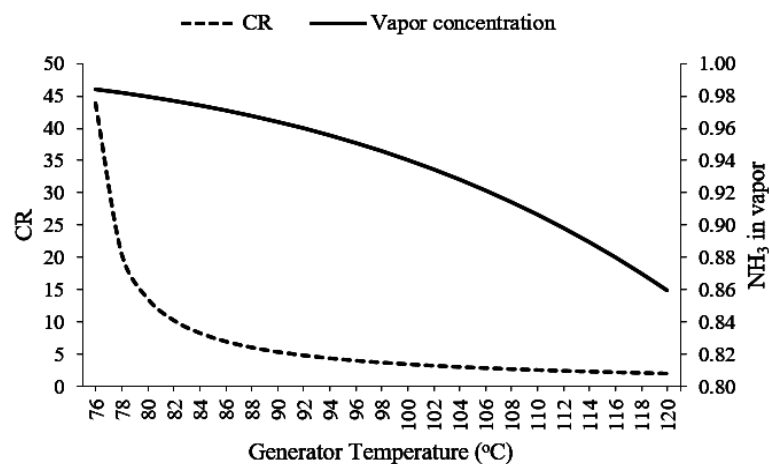
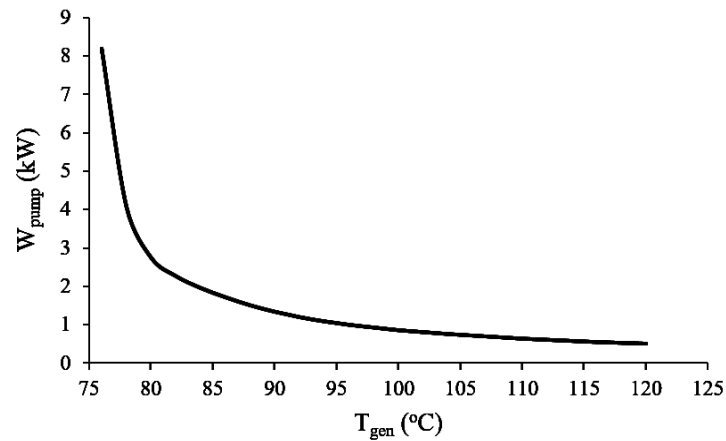**Figure 8.** Variation of NH_3 vapor concentration and CR with T_{gen}.

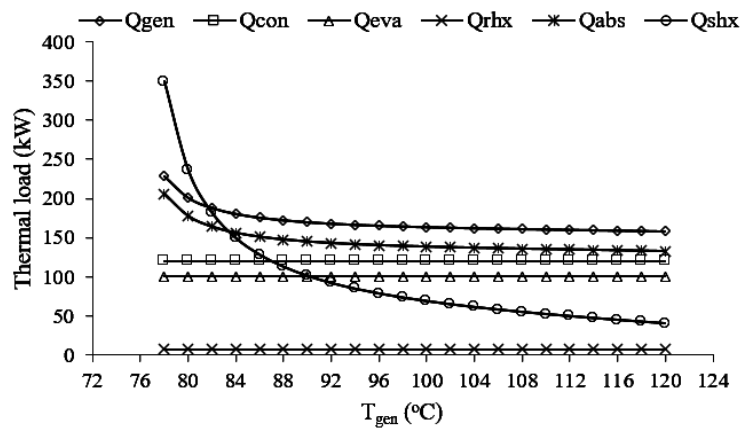**Figure 9.** Effect of T_{gen} on pumping power.

Figure 10. Effects of T_{gen} on Components' thermal loads.

4.3. Effect of Condenser Temperature (T_{con})

The relationships among COP, ECOP and condenser temperature (T_{con}) are implied in Figure 11. T_{con} varies from 20 to 42 °C which corresponds to the change in condensation pressure from 8.555 to 16.4 bar. The decrease in COP is from 0.6208 to 0.10 and in ECOP is from 0.3548 to 0.0467 which is in accordance with the [4,24]. The results can be explained as follows: for constant Q_{eva}, increasing T_{con} means a higher pressure in generator, so less ammonia vapor is released. This situation increases the CR through the generator, absorber and SHX. Consequently, it intensifies the thermal loads in these three components. Results are illustrated in Figures 12 and 13. Following the increase of CR at high T_{con}, required pumping power increases from 1.34 kW at T_{con} of 30 °C to 7.23 kW at T_{con} = 40 °C, as revealed by Figure 14.

Another imperative parameter that is highly affected by changing T_{con} is the generator cut in/off temperature. As T_{con} increases from 20 to 40 °C, the generator pressure increases from 8.555 to 15.52 bar. It leads to increase cut in/off temperature from 62 to 87 °C, as shown in Figure 12.
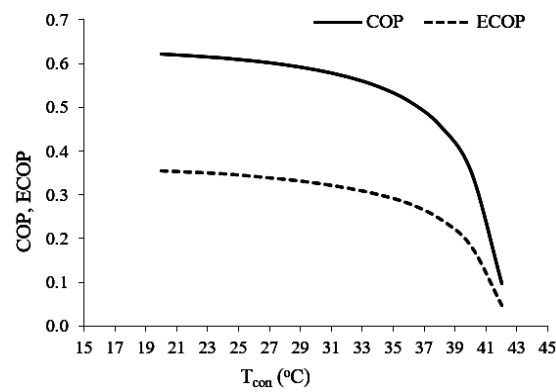
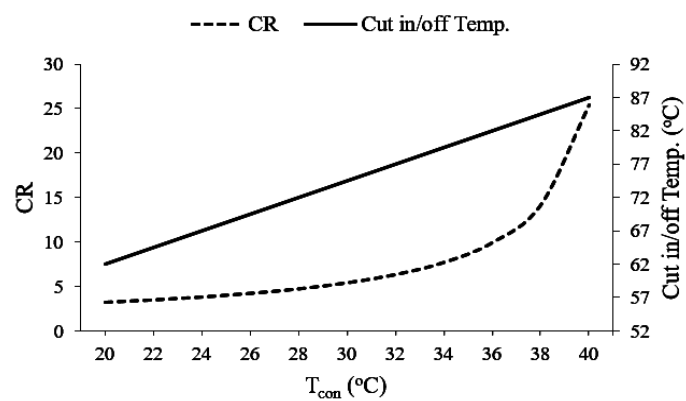**Figure 11.** Effect of T_{con} on COP and ECOP.

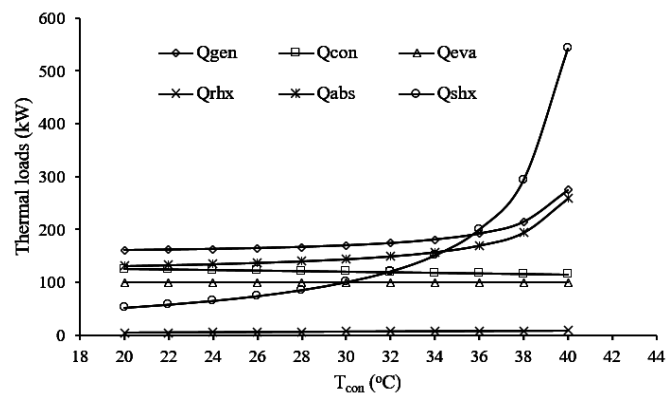**Figure 12.** Variation of cut in/off temperature and CR with T_{con}.

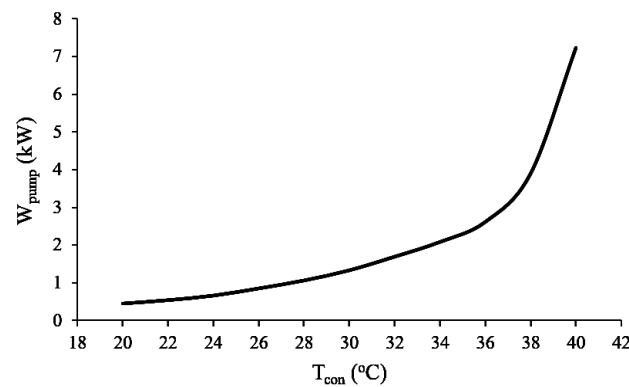**Figure 13.** Variations of Components' thermal loads with T_{con}.

Figure 14. Effect of T_{con} on pumping power.

4.4. Effect of Reflux Ratio (Reflux)

The reflux ratio (Reflux) strongly affects both COP and ECOP as indicated by Figure 15. Increase in Reflux witness an abrupt decrease in COP and ECOP. The effect of Reflux can be explained as follows: for constant Q_{eva}, by increasing Reflux, the vapor leaving rectifier and liquid returning from condenser increases. Hence, more liquid returns to the generator and more vapor must be produced. It implicates that the Q_{gen} must increase and, consequently, the system COP and ECOP decrease, which is in good agreement with the results in [30].

Since the mass flow rates through generator and condenser increase as the Reflux increases, so the thermal loads of these two components increase obviously. The Q_{abs} and Q_{SHX} increase at a lower rate. Figure 16 shows the system components' thermal loads at different reflux ratios. Practically, the Reflux is dependent on rectifier efficiency and ammonia concentration in vapor produced by the generator.
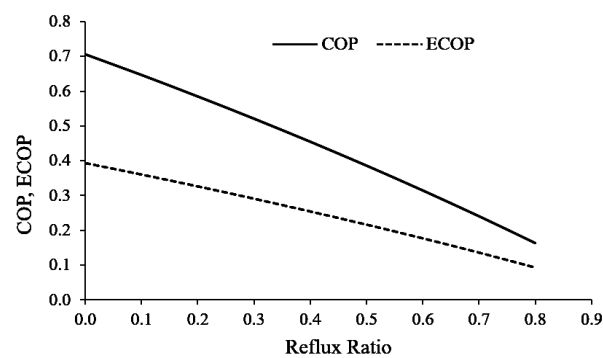

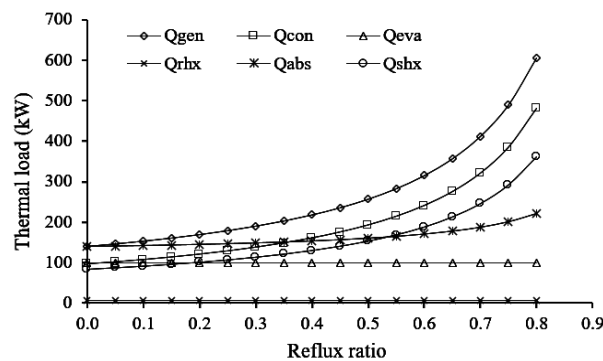**Figure 15.** Effect of reflux ratio on COP and ECOP.

Figure 16. Effect of reflux ratio on components' thermal loads.

4.5. Effect of NH₃ Concentration in Refrigerant (Xᵣ)

In AARSs, the refrigerant entering the evaporator always contains a small fraction of water. This water content in the evaporator, though very less, significantly impacts the system's performance and thermal loads. It occurs due to the reason that complete vaporization of refrigerant cannot be arrived without relatively larger temperature glide in the evaporator. For example, with 2 °C temperature glide, the vapor quality at evaporator exit is 0.9886 for X_r = 0.999 (remaining refrigerant not evaporated). This quality reduces to only 0.8375 for X_r = 0.986 articulating that 16.25% of the refrigerant passes through evaporator without inducing cooling effect. The relation between X_r and vapor quality at evaporator exit is presented in Figure 17. As per the figure, variation of X_r from 0.986 to 0.999, COP increases from 0.4733 to 0.5997 and ECOP increases from 0.2647 to 0.3352. Reason being the refrigerant with a higher concentration can evaporate in evaporator to reach a higher vapor quality (most of the refrigerant evaporated) than the refrigerant with a lower concentration. Therefore, the required refrigerant amount is decreased for constant Q_{eva}. Subsequently, Q_{gen}, Q_{con}, Q_{RHX}, Q_{abs} and Q_{SHX} are effectively lowered with an increase in COP and ECOP, as shown in Figure 18.
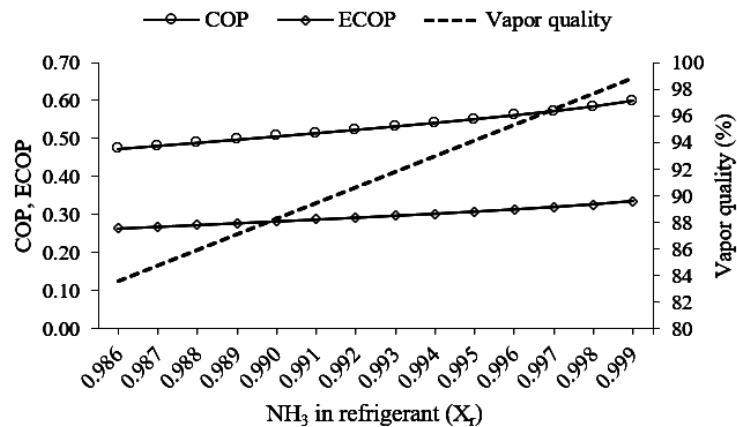

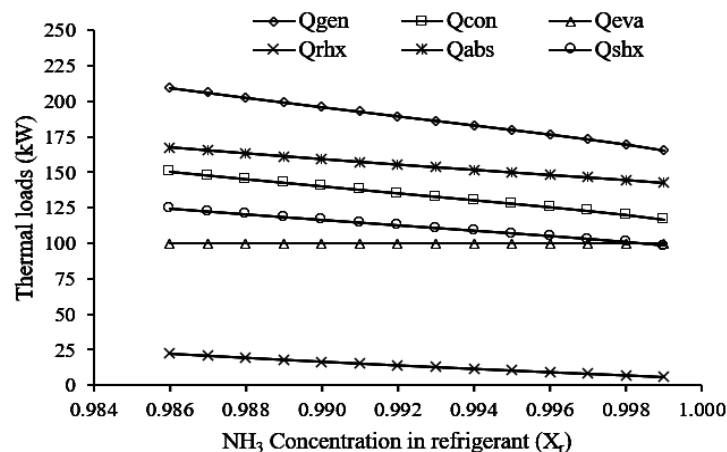**Figure 17.** Effect of X_r on COP, ECOP and vapor quality at evaporator exit.

Figure 18. Variations of thermal loads with X_r.

Another explanation for the improvement in system's performance with increase of X_r is as follows: for same evaporator temperature, higher concentration refrigerant evaporates at slightly higher pressure than the refrigerant with lower concentration. This increases the absorber pressure which allows strong solution to reach a higher concentration, hence the system's performance increases. For example, at evaporator temperature (T_{eva}) −4 °C and X_r = 0.97, the evaporator pressure is 3.58 bar

and strong solution at absorber exit is 0.4767. While at same temperature and X_r = 0.999, the evaporator pressure is 3.685 bar and related X_{ss} is 0.4828.

4.6. Effect of Evaporator Temperature (T_{eva})

Evaporator temperature affects the pressure of evaporator and absorber. The effects of evaporator temperature (T_{eva}) on system's energetic and exergetic performances are illustrated in Figure 19. The T_{eva} varies from −12 to 12 °C which increases the COP from 0.3816 to 0.6613. The higher T_{eva} increases absorber pressure which let the concentration of strong solution (X_{ss}) increase. It consequently decreases the Q_{gen} and leads the COP to increase. For the cause of ECOP, the situation is different: as T_{eva} increases from −12 °C, the ECOP rises to touch its maximum at T_{eva} of −8 °C. This occurs due to decrease in exergy losses in generator, absorber and SHX as their thermal loads are effectively reduced by increase of T_{eva} from −12 to −8 °C (Figure 21). However, with more increase of T_{eva} the ECOP decreases distinctly from 0.3375 to 0.1527. It happens as the evaporator has a lower potential for cooling at a higher temperature. Thus, high increase T_{eva} has a negative effect on ECOP, which corresponds to the results reported in [4,15,31].

On the other hand, since increase in T_{eva} causes an increase in X_{ss}, CR decreases as well as the Q_{gen}, Q_{abs}, Q_{SHX} and Q_{RHX}. However, the Q_{con} slightly increases with the increase in T_{eva}. It takes place because the refrigerant at higher evaporator pressure has a marginally lower vapor quality than that at lower evaporator pressure. This means at a higher T_{eva}, the refrigerant requires more temperature glide to be evaporated completely. Effects of T_{eva} on CR and thermal loads are presented in Figures 20 and 21, respectively. Due to the decrease in CR with increase of T_{eva}, the required pumping power declines from 4.5 kW at T_{eva} = −12 °C to 1 kW at T_{eva} of −2 °C as depicted by Figure 22.
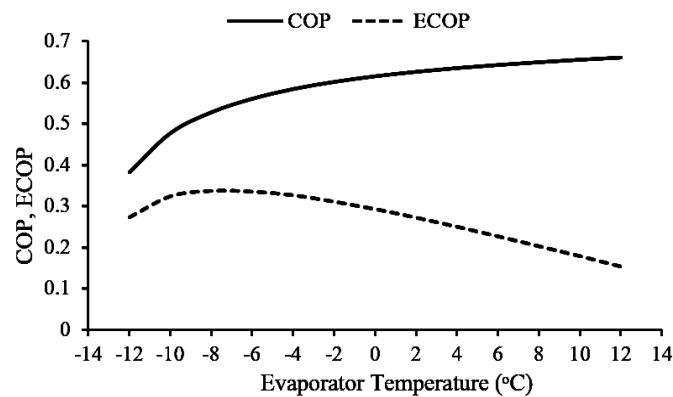

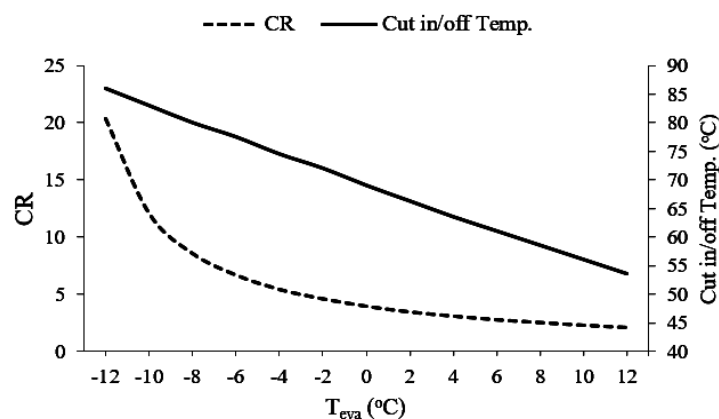**Figure 19.** Effects of T_{eva} on COP and ECOP.

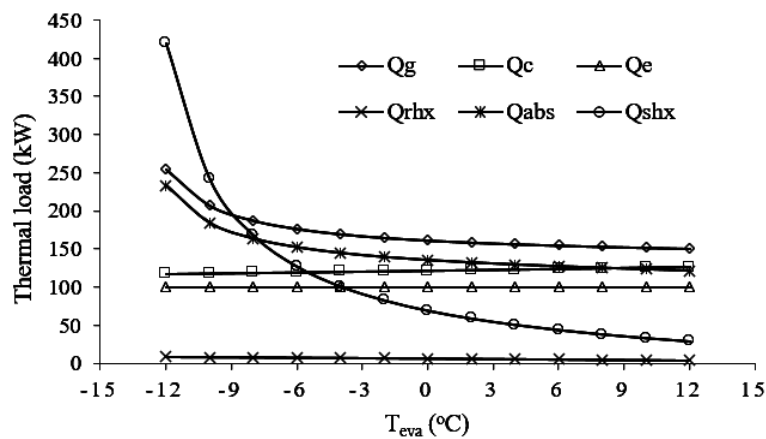**Figure 20.** Effect of T_{eva} on the CR and cut in/off temperature.

Figure 21. Effect of T_{eva} on thermal loads.
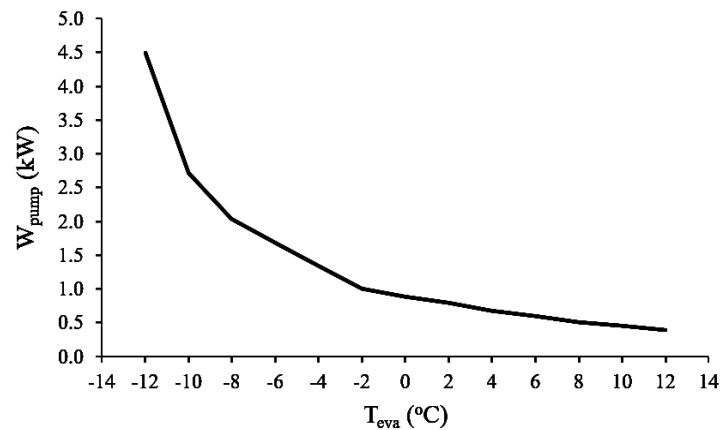

Figure 22. Effect of T_{eva} on pumping power.

As mentioned previously, generator cut in/off temperature depends mainly on X_{ss} and generator pressure. Hence, an increase in evaporator pressure, which lifts the X_{ss} in absorber, has a significant impact on decreasing the cut in/off temperature as presented in Figure 20. Increase in T_{eva} from −12 to 12 °C abruptly decrease the generator cut in/off temperature from 86 to 54 °C.

From these results, it can be comprehended that the increase in T_{eva} has positive effects. The fact is endorsed by the values which increase for COP and decrease for CR, cut in/off temperature, W_{pump} and thermal loads. Only exception is the condenser, which undergoes a small increase in thermal load. At the same time, higher increase in T_{eva} has a negative effect as well since it evidently decreases the ECOP. It is worth mentioning that evaporator temperature is determined generally in accordance to the application requirement, either refrigeration or air-conditioning. Thus, the choice of T_{eva} usually is within a limited range.

4.7. Effect of Evaporator Temperature Glide

In AARSs, required temperature glide to achieve complete vaporization is dependent on water content in the refrigerant and evaporator pressure. For the present cycle, which has a value of 0.998 for X_r, the temperature glide must be kept at about 29 °C to accomplish complete evaporation. Figure 23 shows the effect of temperature glide in evaporator on COP and ECOP.

As interpreted from Figure 23, a small evaporator temperature glide increases both COP and ECOP. At about 2 °C glide, the ECOP reaches its maximum value. Afterwards as the glide increases, the COP continues to increase while the ECOP decreases significantly. This figure also illustrates that complete evaporation could not be attained in evaporator up to 14 °C of glide even though water

in refrigerant is 0.2% only. For the present system, until this glide degree, refrigerant can be 99.5% evaporated. Complete evaporation at evaporator exit was achieved by 29 °C of glide. In the same manner, for constant Q_{eva}, evaporator temperature glide by 2 °C is enough to effectively reduce the Q_{gen}, Q_{con}, Q_{abs}, Q_{RHX} and Q_{SHX}. It should be noticed that further increase in evaporator temperature glide does not produce a remarkable reduction in the thermal loads, as shown by Figure 24. Thus, a small glide of evaporator temperature will improve the system's performance and reduce thermal loads despite the existence of a small amount of liquid refrigerant at the evaporator exit. However, it seems to be compensated since the remaining liquid will be dragged to absorber by vapor flow through RHX. This liquid will be evaporated completely in RHX and its refrigeration effect will be used to sub cool the liquid refrigerant from condenser. This may add more importance for utilizing RHX in situations of low temperature glide, especially when refrigerant concentration is not too high.
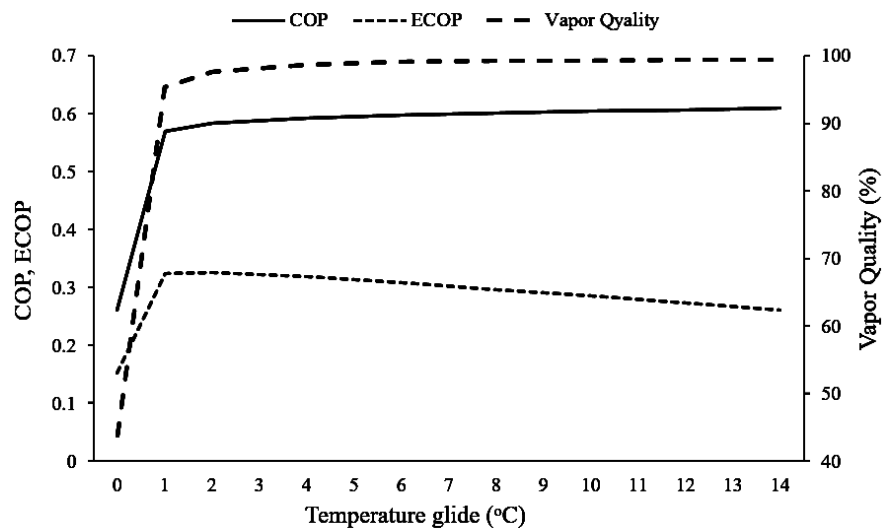

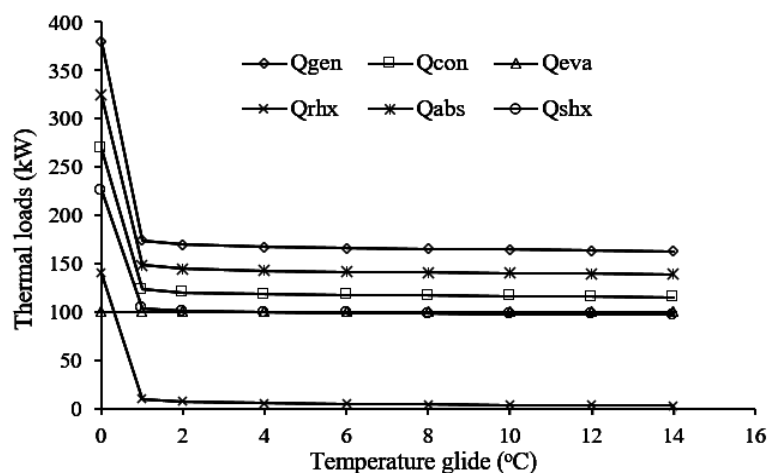**Figure 23.** Effect of temperature glide on COP and ECOP.

Figure 24. Effect of temperature glide on thermal loads.

4.8. Effect of Absorber Temperature (T_{abs})

Increasing T_{abs} directly affects the X_{ss}, which decreases as T_{abs} increases. At high T_{abs}, the X_{ss} approaches that of weak solution and leads CR to increase dramatically. The values of Q_{gen}, Q_{abs} and Q_{SHX} then follow considerable increase with a consequent decrease in COP. In addition, increase of T_{abs} increases the absorber exergy loss as well as the SHX. Resultantly ECOP also decreases. In Figure 25,

the T_{abs} varies from 15 to 42 °C, the COP is decreased from 0.6474 to 0.2851 and ECOP is reduced from 0.3682 to 0.1487 only, which are in a good agreement with results published by Aman et al. [4].
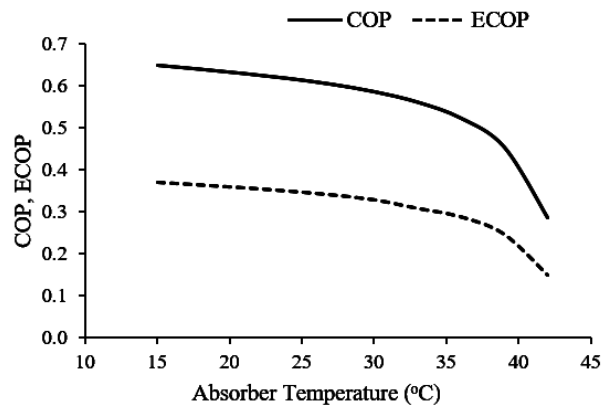

Figure 25. Effect of absorber temperature on COP and ECOP.

For T_{abs} above 40 °C, difference in the concentrations between strong and weak solutions becomes so small, the CR and thermal loads extremely increase and both COP and ECOP rapidly decrease. The effect of T_{abs} on CR and thermal loads are shown in Figures 26 and 27, respectively. As T_{abs} inversely affects the X_{ss} substantially, it will strongly influence generator cut in/off temperature, as illustrated by Figure 26. Increase in T_{abs} from 15 to 42 °C will conspicuously rise the cut in/off temperature from 57 to 88.5 °C. Other negative effect of increasing T_{abs} is the noticeable increase of W_{pump}, as revealed by Figure 28. By increase of T_{abs} from 30 to 42 °C, consumed power by pump sharply increases from 1.34 kW to reach 8.4 kW.
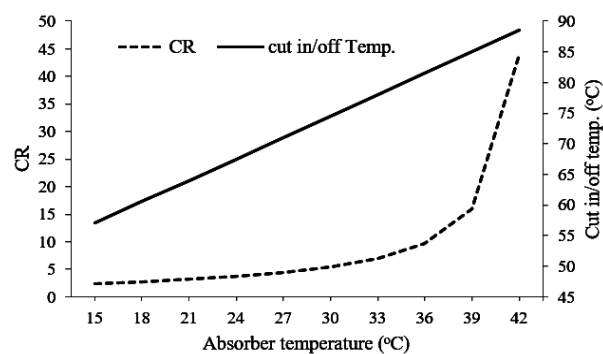

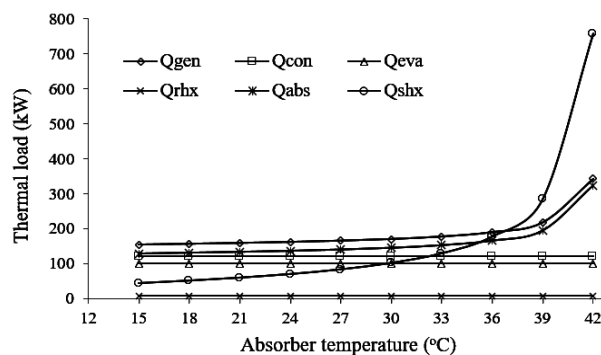**Figure 26.** Effect of T_{abs} on CR and cut in/off Temperature.

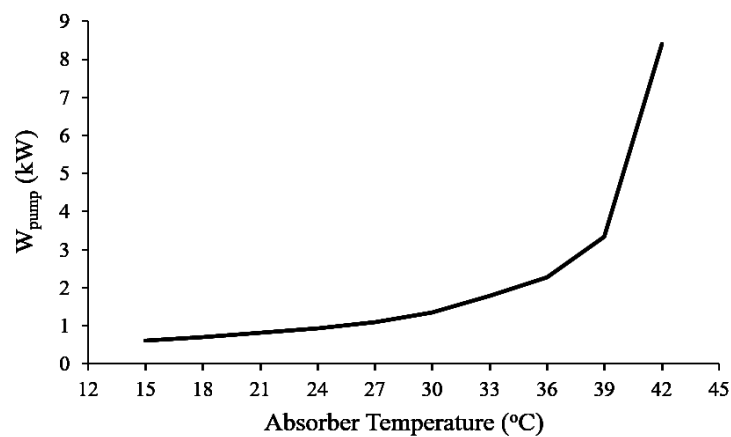**Figure 27.** Effect of T_{abs} on the thermal loads.

Figure 28. Effect of T_{abs} on pumping power.

Usually, T_{abs} and T_{con} are determined by temperature of available cooling medium (water or air). In current study, the condenser and absorber are water cooled. To keep heat transfer rates between working solution and cooling water at required values, the minimum temperature difference must not be less than 6 °C in these components. In other words, for T_{con} and T_{abs} of 30 °C the cooling water temperature must be 24 °C or lower. Otherwise, the condenser and absorber will work at higher temperatures which decrease COP, ECOP and increase the cut in/off temperature, CR and W_{pump}.

4.9. Effect of Solution Heat Exchanger Effectiveness (ε_{SHX})

Solution heat exchanger is regarded as a critical component of the AARS because it affects the system in many aspects. The ε_{SHX} has a major effect on system's performance as displayed in Figure 29 where ε_{SHX} varies from 0.00% (represent no SHX) to 100%. Keeping all other parameters at their base values, the COP increases sharply from 0.1640 to 0.6906 and ECOP increases from 0.0926 to 0.3857.

Rate of heat transfer from the weak solution to strong solution increases with the increase in ε_{SHX}, so the temperature of the strong solution (T_1 in Figure 1) increases while that of the weak solution (T_{13}) decreases. As a result, strong solution enters the generator with a higher temperature and weak solution enters the absorber with a lower temperature. Consequently, both Q_{gen} and Q_{abs} decrease. Figure 30 indicates thermal loads as a function of ε_{SHX} and energetic and exergetic performance increase ratios (PIR) are shown in Figures 31 and 32, respectively. With increase in ε_{SHX}, thermal loads decrease and energetic and exergetic performance improve. As ε_{SHX} value reaches 0.80, the Q_{gen} is reduced by 72%, Q_{abs} is reduced by 75%, COP is increased by 256% and the value of ECOP is increased by 253%. The effectiveness of SHX also has a positive impact on CR, as illustrated by Figure 33, while increase in ε_{SHX} decreases CR. This directly reduces W_{pump}, as uncovered by Figure 34.
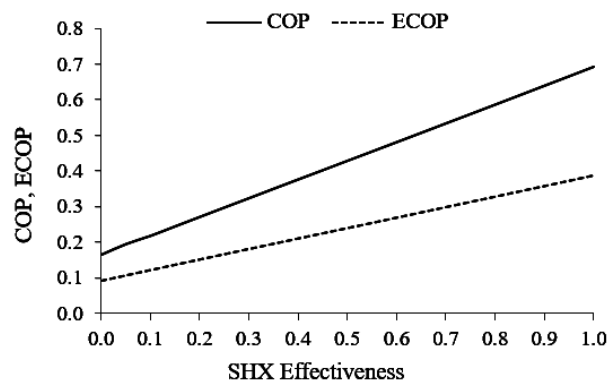

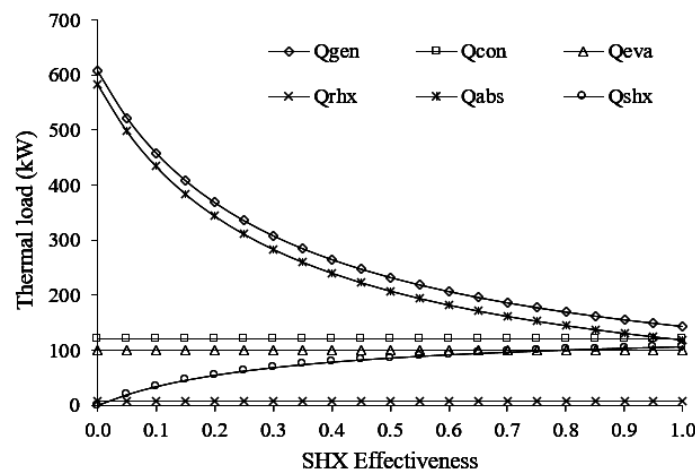**Figure 29.** Effect of ε_{SHX} on COP and ECOP.

Figure 30. Effect of ε_{SHX} on components' thermal loads.
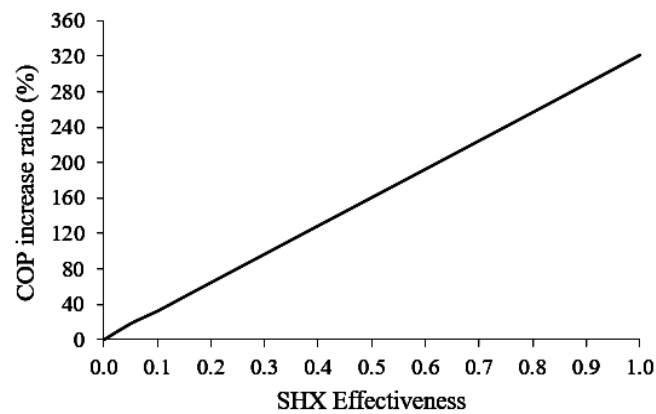
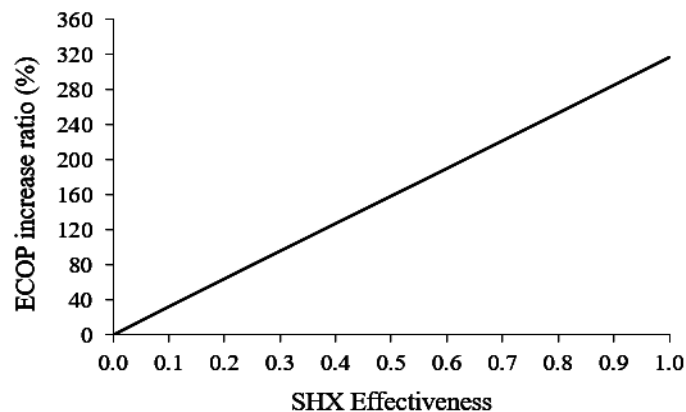**Figure 31.** COP increase ratio as a function of ε_{SHX}.

Figure 32. ECOP increase ratio as a function of ε_{SHX}.

The increase of ε_{SHX} also decreases the generator cut in/off temperature by a reasonable value. For the author's knowledge, relation between ε_{SHX} and generator cut in/off temperature has not been reported before the present study. Figure 33 shows that cut in/off generator temperature can be reduced by more than 10 °C provided a SHX with ε_{SHX} = 0.80 is used. This result can be achieved since SHX with a high effectiveness can preheat the strong solution to approach its saturation temperature

before entering the generator. Later, the entire heat supplied to the generator can be utilized to vaporize ammonia.
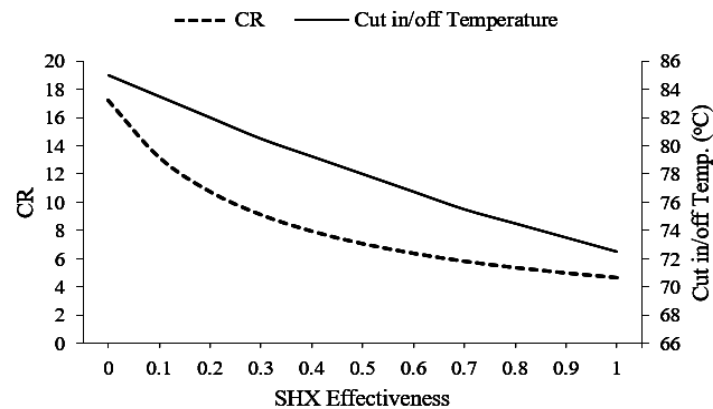

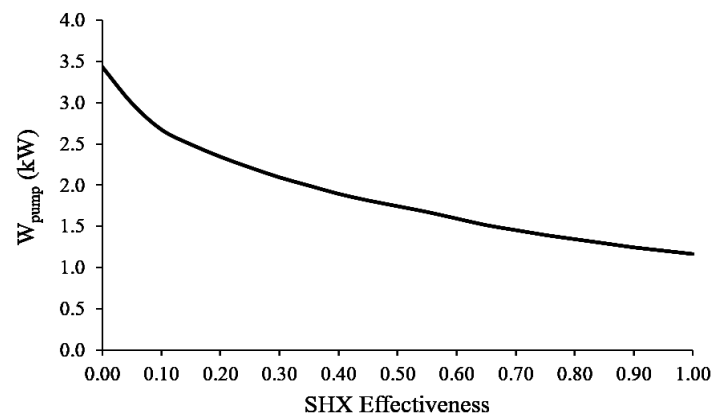**Figure 33.** Effect of ε_{SHX} on the CR and cut in/off temperature.

Figure 34. Effect of ε_{SHX} on pumping power.

In Figures 35 and 36, performance of the system is compared with different ε_{SHX} at different T_{gen}, as shown graphically. By using a SHX with higher effectiveness, maximum COP and ECOP can be achieved at a lower generator temperature. In addition, the differences in values of cut in/off generator temperature show the importance of using a SHX with high effectiveness.
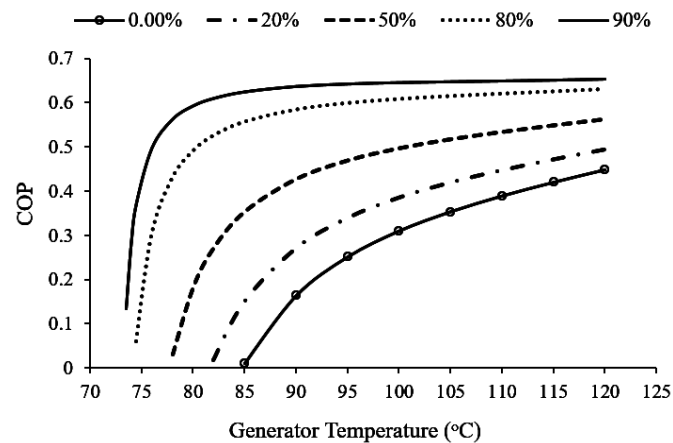

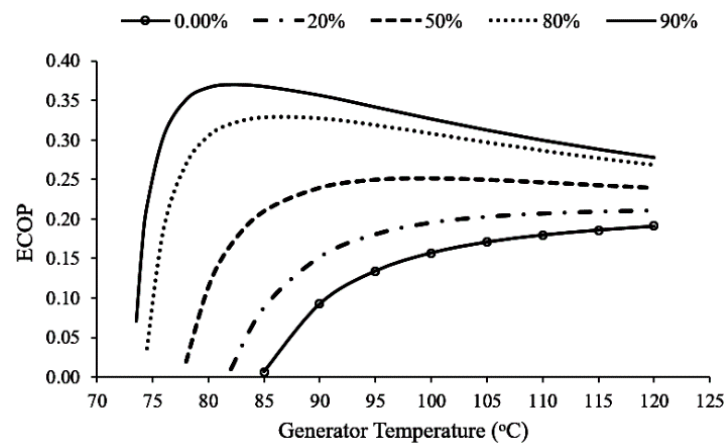**Figure 35.** Variations of COPs with different ε_{SHX} at different T_{gen}.

Figure 36. Variations of ECOPs with different ε_{SHX} at different T_{gen}.

5. Conclusions and Discussion

Main goals of this study are to analyze an ammonia/water ARS for lowering its required driving temperature (cut in/off temperature), and maximizing its performance, keeping in view the first and second laws of thermodynamics. In this regard, energy and exergy analysis of a 100 kW AARS has been performed and effects of all parameters have been investigated. Influences of water content in refrigerant, pressure losses and temperature glide in evaporator have also been considered. The COP, ECOP, CR, required pumping power and different components' thermal loads have been obtained. Following results have been concluded:

- The cut in/off generator temperature is an important parameter in studying AARSs and must be optimized along with other parameters to reduce required driving temperature.
- Results revealed that cut in/off temperature is dependent on the X_{ss}, generator pressure and the ε_{SHX}. It decreases as X_{ss} and ε_{SHX} increase and as the generator pressure decreases. Consequently, all variables (e.g., T_{con}, T_{eva}, T_{abs}, and pressure losses) affecting those three parameters also affect the cut in/off generator temperature.
- In optimization of AARSs, selection of the generator working temperature requires special attention because higher T_{gen} maximize the COP and reduce both CR and electric power required for solution pumping. However, for the systems designed to work at higher T_{gen}, maximum achievable ECOP is a little low.
- Appropriate choice of T_{gen} (without overheating) can increase the ECOP as well as ensure a high ammonia concentration in vapor leaving the generator, and hence reduce the work required by rectifier.
- The temperature of cooling water used to cool both of absorber and condenser has a great impact because both T_{abs} and T_{con} significantly affect the generator cut in/off temperature, COP, ECOP, CR and W_{pump}.
- In evaporator, due to the presence of water in refrigerant, complete evaporation cannot be accomplished without a relatively higher temperature glide. For this reason, while studying AARSs, the assumption of saturated vapor at evaporator exit can lead to misleading results.
- A small temperature glide in evaporator (within 5 °C) will improve both COP and ECOP and reduce the components' thermal loads. However the glide beyond 5 °C will decrease ECOP. On the other hand, increasing the T_{eva} will rise COP and lowers the consumed power by solution pump, but at higher T_{eva} the ECOP decreases sharply.
- In AARSs, the SHX has a prime importance, especially for the systems driven by low temperature heat sources. Employing a SHX with $\varepsilon_{SHX} = 0.8$, the Q_{gen} and Q_{abs} can be reduced by 47% and 53% while the COP and ECOP can be increased by 88% and 87%, respectively. In addition, the CR

can be reduced by 41%, W_{pump} dropped by 61% and the cut in/off temperature can be lowered by about 10 °C.

- For better and reliable analysis, information about electric power consumption by absorption cycle and auxiliaries is pivotal. For standalone solar-driven absorption cooling systems, it is even more crucial. By comparing the results here, it should be noted that for system at base condition, the electric power consumed by auxiliaries (2.3 kW) is higher than that required for solution pumping (1.34 kW). Resultantly, due consideration of the auxiliaries consumption will be more credible in evaluating solar ARSs.

- From the indicated results, it can be judged that an appropriate selection of system working condition values in AARSs, i.e., T_{eva} = −4 °C, and COP and ECOP higher than 0.53 and 0.32, respectively, can be achieved at 90 °C generator temperature. This temperature can be supplied by a low-temperature heat source.

Finally, the comprehensive analysis of AARS presented in this study can be considered as a useful source to observe all parameters that affect cut in/off generator temperature, COP, ECOP, CR, W_{pump} and system thermal loads. These outcomes can facilitate the coming research work in this sector. However, a further study undertaking the effect of water content in refrigerant on exergy loss in each component is needed. Besides, a complete analysis including solar collector, hot water tank and absorption system should also be conducted. These points can be kept in front for future work.

Author Contributions: All authors contributed to this work, Osman Wageiallah developed the used model and wrote the paper. The whole project was supervised by Guo Yanling.

Conflicts of Interest: The authors declare no conflict of interest.

Nomenclature

ARS	Absorption refrigeration system
AARS	Ammonia-water absorption refrigeration system
COP	Coefficient of performance
ECOP	Exergetic coefficient of performance
SHX	Solution heat exchanger
RHX	Refrigerant heat exchanger
X	Mass fraction of ammonia
CR	Circulation ratio
$\dot{m}$	Mass flow rate (kg/s)
$\dot{Q}$	Heat transfer rate (kW)
W	Work rate (kW)
$\dot{E}$	Exergy rate (kW)
h	Specific enthalpy (kJ/kg)
T	Temperature (°C)
E	Specific exergy (kJ/kg)
Reflux	Reflux ratio
P	Pressure (kPa)
Subscripts	
ss	Strong solution (strong in refrigerant)
r	Refrigerant
in	Going in
out	Going out
o	Reference state
dest	Destroyed
gen	Generator
rect	Rectifier

con	Condenser
eva	Evaporator
abs	Absorber
pump	Solution pump

Greek symbols

ε	Effectiveness
Δ	Difference in any quantity
ν	Specific volume of solution (m^3/kg)
η	Efficiency

References

1. Sarbu, I.; Sebarchievici, C. General review of solar-powered closed sorption refrigeration systems. *Energy Convers. Manag.* **2015**, *105*, 403–422. [CrossRef]

2. Fong, K.; Chow, T.T.; Lee, C.K.; Lin, Z.; Chan, L. Comparative study of different solar cooling systems for buildings in subtropical city. *Solar Energy* **2010**, *84*, 227–244. [CrossRef]

3. Kaygusuz, K. Energy, electricity and socioeconomic transformation of rural regions in developing countries. *Energy Sources B Econ. Plan. Policy* **2011**, *6*, 384–394. [CrossRef]

4. Aman, J.; Ting, D.-K.; Henshaw, P. Residential solar air conditioning: Energy and exergy analyses of an ammonia–water absorption cooling system. *Appl. Therm. Eng.* **2014**, *62*, 424–432. [CrossRef]

5. Mohammed, O.W.; Yanling, G. Estimation of Diffuse Solar Radiation in the Region of Northern Sudan. *Int. Energy J.* **2017**, *16*, 163–172.

6. Anand, S.; Gupta, A.; Tyagi, S. Solar cooling systems for climate change mitigation: A review. *Renew. Sustain. Energy Rev.* **2015**, *41*, 143–161. [CrossRef]

7. Anand, S.; Gupta, A.; Tyagi, S. Renewable energy powered evacuated tube collector refrigerator system. *Mitig. Adapt. Strateg. Glob. Chang.* **2014**, *19*, 1077–1089. [CrossRef]

8. Abu-Ein, S.Q.; Fayyad, S.M.; Momani, W.; Al-Bousoul, M. Performance analysis of solar powered absorption refrigeration system. *Heat Mass Transf.* **2009**, *46*, 137–145. [CrossRef]

9. Gebreslassie, B.H.; Guillén-Gosálbez, G.; Jiménez, L.; Boer, D. Design of environmentally conscious absorption cooling systems via multi-objective optimization and life cycle assessment. *Appl. Energy* **2009**, *86*, 1712–1722. [CrossRef]

10. Siddiqui, M.; Said, S. A review of solar powered absorption systems. *Renew. Sustain. Energy Rev.* **2015**, *42*, 93–115. [CrossRef]

11. Trott, A.R.; Welch, T. *Refrigeration and Air Conditioning*; Butterworth-Heinemann: Oxford, UK, 2000.

12. Wu, W.; Wang, B.; Shi, W.; Li, X. An overview of ammonia-based absorption chillers and heat pumps. *Renew. Sustain. Energy Rev.* **2014**, *31*, 681–707. [CrossRef]

13. Dalkılıç, A.S.; Celen, A.; Çebi, A.; Wongwises, S. Effect of Refrigerant Type and Insulation Thickness on Refrigeration Systems of Land and Sea Vehicles. *Stroj. Vestnik-J. Mech. Eng.* **2016**, *62*, 252–259. [CrossRef]

14. Kong, D.; Liu, J.; Zhang, L.; He, H.; Fang, Z. Thermodynamic and experimental analysis of an ammonia-water absorption chiller. *Energy Power Eng.* **2010**, *2*, 298. [CrossRef]

15. Sözen, A.; Altıparmak, D.; Usta, H. Development and testing of a prototype of absorption heat pump system operated by solar energy. *Appl. Therm. Eng.* **2002**, *22*, 1847–1859. [CrossRef]

16. Fernández-Seara, J.; Sieres, J. The importance of the ammonia purification process in ammonia-water absorption systems. *Energy Convers. Manag.* **2006**, *47*, 1975–1987. [CrossRef]

17. Gadalla, M.A.; Ibrahim, T.A.; Hassan, M.A. Performance characteristics of an ammonia-water absorption heat pump system. *Int. J. Energy Res.* **2013**, *37*, 1917–1927. [CrossRef]

18. Bogart, M. Pitfalls in ammonia absorption refrigeration. *Int. J. Refrig.* **1982**, *5*, 203–208. [CrossRef]

19. Fernández-Seara, J.; Sieres, J. Ammonia-water absorption refrigeration systems with flooded evaporators. *Appl. Therm. Eng.* **2006**, *26*, 2236–2246. [CrossRef]

20. Táboas, F.; Bourouis, M.; Vallès, M. Analysis of ammonia/water and ammonia/salt mixture absorption cycles for refrigeration purposes in fishing ships. *Appl. Therm. Eng.* **2014**, *66*, 603–611. [CrossRef]

21. Bejan, A.; Tsatsaronis, G. *Thermal Design and Optimization*; John Wiley & Sons: Hoboken, NJ, USA, 1996.

22. Hepbasli, A. A key review on exergetic analysis and assessment of renewable energy resources for a sustainable future. *Renew. Sustain. Energy Rev.* **2008**, *12*, 593–661. [CrossRef]

23. Mohammed, O.W.; Yanling, G. Yearly Energetic and Exergetic Performance of Solar Absorption Refrigeration System in the Region of Northern Sudan. *Int. Energy J.* **2017**, *17*, 141–154.

24. Sözen, A. Effect of heat exchangers on performance of absorption refrigeration systems. *Energy Convers. Manag.* **2001**, *42*, 1699–1716. [CrossRef]

25. Palomba, V.; Aprile, M.; Motta, M.; Vasta, S. Study of sorption systems for application on low-emission fishing vessels. *Energy* **2017**, *134*, 554–565. [CrossRef]

26. Woudstra, N.; van der Stelt, T.P. *Cycle-Tempo: A Program for Thermodynamic Modeling and Optimization of Energy Conversion Systems*; Delft University of Technology: Delft, The Netherlands, 2002.

27. Le Lostec, B.; Galanis, N.; Millette, J. Experimental study of an ammonia-water absorption chiller. *Int. J. Refrig.* **2012**, *35*, 2275–2286. [CrossRef]

28. Mendes, L.; Collares-Pereira, M. A solar assisted and air cooled absorption machine to provide small power heating and cooling. In Proceedings of the International Sorption Heat Pump Conference, Munich, Germany, 24–26 March 1999; pp. 129–136.

29. Gebreslassie, B.H.; Medrano, M.; Mendes, F.; Boer, D. Optimum heat exchanger area estimation using coefficients of structural bonds: Application to an absorption chiller. *Int. J. Refrig.* **2010**, *33*, 529–537. [CrossRef]

30. Fernández-Seara, J.; Sieres, J.; Vázquez, M. Distillation column configurations in ammonia-water absorption refrigeration systems. *Int. J. Refrig.* **2003**, *26*, 28–34. [CrossRef]

31. Ataer, Ö.E.; Göğüs, Y. Comparative study of irreversibilities in an aqua-ammonia absorption refrigeration system. *Int. J. Refrig.* **1991**, *14*, 86–92. [CrossRef]